Cyclic dinucleotides bind the C-linker of HCN4 to control channel cAMP responsiveness

Authors: Lolicato[1*], M., Bucchi[1*], A., Arrigoni[1], C., Zucca[1], S., Nardini[1], M., Schroeder[2], I., Simmons[3], K., Aquila[1], M., DiFrancesco[1], D., Bolognesi[1,4], M., Schwede[5], F., Kashin[5], D., Fishwick[3], C.W.G, Johnson[3], A.P. , Thiel[2], G., Moroni[1,4,§] A.

Affiliations: [1]Department of Biosciences, University of Milan, Italy; [2]Department of Biology, Technische Universität-Darmstadt, Germany, [3]School of Chemistry, University of Leeds, UK; [4] Istituto di Biofisica, Consiglio Nazionale delle Ricerche, Milan, Italy; [5]BIOLOG Life Science Institute, Forschungslabor und Biochemica-Vertrieb GmbH D-28199 Bremen, Germany.

*These Authors equally contributed to the work.

§Corresponding author: Anna Moroni, Dept. of Biosciences, Via Celoria 26, 20133 Milano, Italy, anna.moroni@unimi.it, tel +390250314826, fax +390250314815

Autonomic regulation of heart rate is largely mediated by the effect of cAMP on the pacemaker current I_f, driven by hyperpolarization-activated cyclic nucleotide-gated (HCN) channels. cAMP

enhances HCN open probability by binding to the CNBD (cyclic nucleotide binding domain). The C-linker transmits the cAMP-induced conformational change from the CNBD to the pore and is thus considered a passive element in the opening transition. Here we report the finding of an allosteric binding site in the C-linker of HCN4 that implies a regulatory function of this domain. By structural and functional analysis we show that cyclic dinucleotides, an emerging class of second messengers in mammals, bind to this C-linker pocket (CLP) and antagonize cAMP regulation of HCN4 channels. Accordingly, cyclic dinucleotides prevent cAMP regulation of I_f in sinoatrial-node myocytes, reducing heart rate by 30%. The same effect is attained by Compound 11, a molecule selected by virtual docking to the CLP. Occupancy of the CLP hence constitutes an efficient mechanism to prevent β-adrenergic stimulation on I_f. Our results highlight the regulative role of the C-linker in HCN4 and identify an isoform-specific drug target within the HCN family. Furthermore, these data extend the signaling scope of cyclic dinucleotides in mammals, beyond their first reported role in innate immune system.

Introduction

The "funny" current (I_f) of cardiac pacemaker myocytes is an inward current activated by hyperpolarization of membrane voltage and controlled by intracellular cAMP[1]. Being activated and inhibited by β-adrenergic and muscarinic M2 receptor stimulation, respectively, I_f represents a basic physiological mechanism mediating autonomic regulation of heart rate and constitutes an ideal target for the pharmacological control of cardiac activity. The molecular determinants of I_f are the Hyperpolarization-activated cAMP-gated (HCN) channels[2,3]. In these proteins, the transmembrane pore is connected at the N terminus to a voltage sensor domain and at the C-terminus to a cytosolic cyclic-nucleotide-binding domain (CNBD). The C-linker, an α-helix folded domain of 90 amino acids, connects the CNBD to the pore. Structural studies showed that the cytosolic C-terminal fragment (C-linker + CNBD) assembles as a 4-fold symmetric tetramer in which the primary subunit interactions are provided by the linkers. The C-linkers form a ring in which the first two helices of one subunit (A' and B') form a helix-turn-helix motif that rests as an "elbow" on the "shoulder" formed by the second two helices, C' and D', of the neighboring subunit[4]. Enhancement of channel open probability by cAMP reflects the transition from the cAMP-unbound to the bound conformation of the

CNBD that induces a centrifugal rearrangement of the C-linkers with the shoulders twisting away from the elbows[5]. This movement in turn stabilizes the open conformation of the pore. Given the critical role of the C-linker in HCN channel modulation by ligands, it is interesting to note that this linker is missing in the prokaryotic HCN homolog MlotiK, in which the CNBD directly modulates the pore[6,7]. A direct versus indirect coupling of the CNBD to the pore in different cyclic nucleotide gated channels raises the question of whether the C-linker plays in HCN channels a passive or an active role in the transduction of the cAMP signal. It is reasonable to speculate that the increase in structural complexity in eukaryotic HCN channels over the bacterial homolog allowed some additional modes of regulation, which are not present in channels which lack C-linkers. We have now identified a novel binding site, within the C-linker of HCN4, which is part of a mechanism that effectively prevents cAMP activation in this isoform. The C-linker hence adds an additional layer of complexity to provide fine tuning of the activity of the HCN4 channel. Somewhat surprisingly, the lead players of this control mechanism are cyclic dinucleotides, e.g. signaling molecules, which were long believed to function exclusively in bacteria[8]. However after the recent discovery of these molecules in eukaryotes[9] it became evident that they also function as second messengers in metazoa[10,11] although their known scope of their activity has so far been restricted to the immune system.

Results

The native I_f current is modulated by cAMP and, albeit with a lower affinity, also by cGMP[12]. In order to understand the molecular details of the interaction of cGMP with its binding site in the CNBD, we solved the structure of the C-linker and CNBD (CL-CNBD) of HCN4, the main isoform of the cardiac pacemaker[13], in complex with cGMP. The structure unexpectedly showed two bound cGMP molecules per monomer. The first cGMP was located in the "canonical" CNBD binding site[4] while the second was found at the interface between the C-linker and the CNBD, in what we refer to as the C-linker pocket (CLP) (Fig.1a,b). In all four HCN4 protomers of the crystal asymmetric unit, a cGMP molecule was modeled in the electron density at the CLP and the structure was successfully refined at 2.7Å resolution, with full atomic occupancy and average B factors comparable to those of adjacent protein residues (Supplementary Table 1). Notably, no electron density was present in the CLP for crystals grown in the presence of cAMP[14]. The CLP-bound cGMP

molecule is in a *syn* conformation and, by interacting with residues of helix B', B'-C' linker and helix C', bridges the "elbow" and the "shoulder" domain of each subunit[4]. In addition, it interacts with strand β8 of the CNBD (Fig.1c, Supplementary Table 2a). Moreover, several items of structural evidence of cGMP selectivity were found: the hydrogen bond between F564 amide (main chain) nitrogen and oxygen O6 of c-GMP would not be possible because in cAMP oxygen O6 is replaced by an amino group (N6); the polar contact between the residue Y559 and the N2 nitrogen atom, can only occur with cGMP since the cAMP molecule lacks that atom. CyclicGMP was not observed in the CLP of HCN1 (our unpublished results) and HCN2 [4] despite conservation of the residues that directly interact with the molecule. Alignment of the three sequences (Supplementary Fig.1) highlights the occurrence of several amino acid substitutions in the CLP region that can result in a different local structure of the CLP. Superposition of the Cα chains among HCN isoforms indeed reveals a marked mismatch in the Cα backbone of the C'- and D'-helices in HCN4 relative to HCN1/HCN2, both in the cGMP and in the cAMP bound forms (Supplementary Fig. 2a and 2b).

In spite of structural evidence for binding, application of cGMP to HCN4 channels expressed in HEK293T cells did not exhibit any effect on channel function that could be related to occupancy of the CLP. Addition of cGMP to inside-out patches increased HCN4 currents and shifted the voltage for half maximal activation ($V_{1/2}$) towards positive values (Supplementary Fig. 3a), an effect that can be attributed to cGMP binding to the canonical CNBD site. In fact the cGMP binding mode to this pocket matches that of other HCN isoforms (Supplementary Fig. 2c and Supplementary Table 2b). Hill-plot fitting of the dose-response curve yields values of 13.2 μM for half maximal concentration ($k_{1/2}$), and 0.72 for the Hill coefficient (*n)* (Supplementary Fig. 3b), which are quite similar to previously reported values for I_f[12]. Furthermore, application of cGMP at $\geq$ 2.5 mM, e.g. concentrations used for crystallization, did not reveal a second component in Hill plots that could be attributed to a secondary binding site (Supplementary Fig. 3c,d).

After excluding a functional relevance of cGMP binding to the CLP, further analysis revealed that the pocket is sufficiently wide and accessible to bind a molecule about twice the size of cGMP (Fig.1d). Since recent studies identified cyclic di-(3',5')-guanosine monophosphate (c-di-GMP, Supplementary Fig. 4) as a second messenger in eukarya [9,11], we tested c-di-GMP binding to the CLP of HCN4 *via* molecular docking simulation. One of the best docking poses in terms of estimated free energy of binding showed one sugar

ring/nucleotide moiety of the c-di-GMP occupying a similar position (although with a slightly different orientation) as the CLP-bound cGMP in the crystal structure, with the second half of the docked molecule being docked in the charged surface cleft (Fig. 1e,f). Functional tests on HCN4 currents showed a striking result. While addition of c-di-GMP (100 μM) in the pipette did not affect the voltage-dependence of HCN4 currents measured in whole cell, the activation curve in the presence of c-di-GMP being indistinguishable from the control (Fig. 2a), completely opposite results were obtained in the presence of cAMP (15 μM). In this case, c-di-GMP completely reversed (i.e. back-shifted) the positive shift of 18 mV induced by saturating cAMP on the activation curve (Fig. 2b, Supplementary Fig. 5a,b). Figure 2c shows the back shift (in mV) as a function of c-di-GMP concentrations. Hill-plot fitting yielded values of 1.8 μM for $k_{1/2}$ and 1.2 for *n*. To confirm the direct action of c-di-GMP, we tested the molecule in the inside-out configuration (Fig. 2d). Addition of c-di-GMP (100 μM) instantaneously and efficiently inhibited the increase in current induced by cAMP, fully reversing the shift of 17 mV induced by cAMP on $V_{1/2}$ (inset). Raising the cAMP concentration to 1 mM did not change the effect of c-di-GMP on current and activation curve (Supplementary Fig. 5c,d). This excludes competition of the two molecules for the same binding pocket. Indeed, attempts to dock c-di-GMP into the cAMP-free "canonical" pocket in the CNBD of HCN4 indicated no binding, probably because of the excessive size c-di-GMP. In order to exclude the possibility that the effect of c-di-GMP is mediated by the interaction with its known receptor STING[11], we confirmed by western blot that our heterologous expression system, HEK293T cells, does not express STING protein at detectable levels, neither in basal conditions nor when transfected with HCN4 channels (Supplementary Figure 6**a**). Moreover, as an additional control, we checked whether the effect of c-di-GMP on HCN4 currents was cAMP-specific. To this end, we tested the effect of c-di-GMP in the presence of saturating cGMP (1 mM). Data reported in panel **b** of Supplementary Figure 6 indicates full recovery by c-di-GMP from the cGMP-induced shift in the activation curve of HCN4.

To confirm specific binding of c-di-GMP to the CLP, we searched for site-directed mutations that would abolish or alter the c-di-GMP effect. We selected four key residues (Y559, F564, E566, R680), which line the pocket occupied by the sugar ring/nucleotide moiety of both the cGMP in the crystal structure and of the docked c-di-GMP (Fig. 1c,e). Mutation of any one of these four residues altered the channel response to c-di-

GMP, as shown by the values of $V_{1/2}$ measured in control, cAMP and cAMP + c-di-GMP (Figure 2e). In particular the HCN4 R680E single site mutant proved totally insensitive to c-di-GMP, while its other properties (basal position of $V_{1/2}$ and cAMP-induced shift) remained undistinguishable from wt. This phenotype strongly supports the specific interaction of c-di-GMP with the CLP, ruling out the possibility that c-di-GMP binds to the canonical cyclic nucleotide binding site in the CNBD. In addition, we tested on the wt channel the effect of two control substances, Guanosine-5'-triphosphate **(**GTP, 1 mM) and G5'-Phosphoguanylyl- (3' − 5')-guanosine (pGpG) (100 μM), respectively the precursor and the first metabolic degradation product of c-di-GMP. No effect on the cAMP-induced shift was observed in both cases (data not shown), confirming that the HCN4 pocket is rather specific for c-di-GMP.

Docking experiments showed that c-di-GMP would not bind to other isoforms e.g. HCN1 and HCN2. Although the predicted binding pocket has a high sequence homology, the difference in orientation of E566 (HCN4 numbering) may be a key factor in preventing binding of c-di-GMP to HCN1 and 2 because of a potential steric clash between this residue making and of the phosphate groups of c-di-GMP (Supplementary Figure YY). When c-di-GMP was tested at saturating concentration on human HCN1 and HCN2 channels expressed in HEK293T cells (Fig. 2f), neither of the two channels were affected, confirming that the CLP is specific for the HCN4 isoform.

We next tested other cyclic dinucleotides on HCN4: the bacterial c-di-AMP[8] (cyclic di-(3',5')-adenosine monophosphate), and two linkage isomers of cyclic GMP-AMP (cGAMP), the bacterial 3'3'-cGAMP (c[G(3',5')pA(3',5')p])[15] and the mammalian 2'3'-cGAMP (c[G(2',5')pA(3',5')p])[16-18] (Supplementary Fig.4). All tested cyclic dinucleotides behaved as c-di-GMP, back-shifting $V_{1/2}$ to the control values, in the presence of cAMP (Fig. 2f and Supplementary Fig. 7).

We have extended the analysis on 2'3'-cGAMP, since this is, so far, the only cyclic dinucleotide known to be synthesized by mammals. Molecular docking simulation of 2'3'-cGAMP to HCN4 predicted the dinucleotide would bind in the same pocket as c-di-GMP but in a slightly different orientation. However it would still make interactions with the same key residues as identified for c-di-GMP (Supplementary Figure 8a). When we determined the dose-response curve of the effect of 2'3'-cGAMP on HCN4 currents (Supplementary Figure 8b), we found a $k_{1/2}$ value of 114 nM, which is about 16 times lower than that for c-di-GMP.

Interestingly, the same difference in affinity, nanomolar for the mammalian 2'3'-cGAMP vs. micromolar for the bacterial c-di-GMP has also been reported for STING.

In conclusion, our findings point to a general mechanism whereby cyclic dinucleotides, either endogenous or exogenous, would act as allosteric regulators of the human HCN4 pacemaker channel. Since HCN4 is the main HCN isoform expressed in the cardiac pacemaker[13], we next tested the effect of cyclic dinucleotides on the native I_f current recorded in myocytes acutely isolated from mouse SAN (Fig. 3a). Sample current traces were recorded in the absence and in the presence of c-di-GMP (100 μM), or 2'3'-cGAMP (100 μM), and without (top), or with cAMP (10 μM, bottom), in the pipette solution. Both c-di-GMP and 2'3'-cGAMP shifted $V_{1/2}$ of I_f negative (Fig. 3b,c) (by 5 and 5.3 mV, respectively, see Supplementary Table 3) because both compounds inhibit the shift induced by basal cAMP concentrations. Accordingly, the positive shift in $V_{1/2}$ generated by the addition of cAMP (see Supplementary Table 3) is partially or completely inhibited by c-di-GMP (b, shift = 4.9 mV) and 2'3'-cGAMP (c, shift = 0.8 mV). The effect of c-di-GMP and 2'3'-cGAMP on I_f mimics a cholinergic type of action[17], and hence predicts that both compounds reduce cardiac automaticity. When tested on the activity of single SAN cells, 2'3'-cGAMP indeed substantially decreased the spontaneous rate of these cells, when added at 100 μM via the pipette (Fig. 4d). A 5.3 mV shift in $V_{1/2}$ and a 29% decrease in heart rate from the control of 6.7 ± 0.8 Hz (n = 4) to 4.7 ± 0.3 Hz (n = 5) ($P < 0.05$) (Fig. 4d) correspond to the effects of physiological concentrations of acetylcholine (about 30 nM)[17].

Next we set up a search for synthetic molecules, which would bind HCN4 CLP and modulate channel function. To this aim we exploited libraries of low molecular weight compounds through *in silico* screening. Eleven compounds, structurally unrelated to cyclic dinucleotides, were selected for their high predicted binding affinity and tested on HCN4 currents. The compound N'-biphenyl-2-yl-N-[1-(3-cyanobenzyl)piperidin-4-yl]-N-(pyridin-3-ylmethyl)urea (IUPAC name, CAS number 909664-41-1, hereafter called C11 (Supplementary Fig. 4) had the strongest effect, completely abolishing the cAMP-induced shift in $V_{1/2}$ (Fig. 4a,b). The dose-response curve (Fig. 4c) yielded a $k_{1/2}$ of 0.42 ± 0.11 μM, *i.e.* 4-fold higher apparent affinity than c-di-GMP. Mutation of the interaction sites in the CLP identified by docking (Fig. 4d,e) indeed altered the response of HCN4 to C11, supporting the prediction that C11 binds in the CLP (Fig.

4f). C11 did not affect human HCN2 channels expressed in HEK293T cells (Fig.4f), confirming that the CLP is specific of the HCN4 isoform.

When tested on the native I_f current in the absence and in the presence of cAMP (Figure 4g), C11 shifted $V_{1/2}$ of I_f negative by 5.9 mV (Fig. 4h, Supplementary Table 3), efficiently inhibiting the shift induced by basal cAMP concentrations. The positive shift in $V_{1/2}$ induced by the addition of cAMP was fully inhibited by C11 (shift = 0.3 mV). Again, when tested on the activity of single SAN cells, C11 decreased the spontaneous rate of single SAN cells by 30% (from the control of 7.6 ± 0.4 (n = 7) to 5.4 ± 0.5 Hz (n = 6) ($P < 0.05$)) (Fig. 4i), effectively mimicking the action of endogenous acetylcholine on heart rate.

Discussion

The combination of structural, biochemical and functional data reported here shows that the C-linker of HCN4 hosts a regulatory binding site, the CLP, which controls the effect of cAMP on channel open probability. This mechanism is specific for HCN4 and not effective in HCN1 and HCN2. Since HCN4 is the main isoform of the cardiac I_f, occupancy of CLP by ligand molecules indeed prevents β-adrenergic stimulation on the native current, mimicking the physiological effect of acetylcholine. Even though the control of the responsiveness of HCN channels to cAMP in the heart is reported here for the first time, a down regulation of the cAMP effect seems to be a general requirement for fine-tuning of HCN channel activity. In the brain, where these channels control neuronal excitability and information processing, their response to cAMP is down regulated by the beta subunit TRIP8b[18,19]; this cytoplasmic protein co-assembles with HCN channels and inhibits channel opening by antagonizing the effect of cAMP. TRIP8b allosterically competes with cAMP for channel opening and shifts the activation curve to more negative potential; the same allosteric competition occurs when ligands bind to the CLP in HCN4. The modulation by CLP is therefore functionally but not structurally comparable to that of TRIP8b. Since TRIP8b is exclusively expressed in the brain, this modulator is not relevant for the control of cardiac pacemaking activity. The CLP-based mechanism described here, remarkably specific for HCN4, therefore constitutes a relevant way to down regulate the response of I_f to cAMP in sinoatrial-node.

The observation that occupancy of the CLP prevents cAMP modulation sheds light on the allosteric coupling between the CNBD and the pore in HCN proteins[5]. Ligand binding to the CLP seems to act as a lock, hampering the movement of the C-linker and preventing the transmission of the conformational change from the CNBD to the pore[5]. The CLP is strategically located between two mobile regions of the C-linker, the "elbow" and "shoulder", a location typically occupied by allosteric effectors in many unrelated proteins. When the cAMP-bound CNBD initiates the conformational changes leading to channel activation, the ligand-bound CLP prevents structural rearrangement therefore favoring the resting configuration of the C-linker. Mutagenesis analysis further supports the finding that the CLP is located in a crucial position that controls gating properties of the channel. Three out of four mutations introduced in the CLP in this study (Y559T, F564T, E566K), resulted in channels with altered gating properties (altered basal value of $V_{1/2}$ and/or altered response to cAMP) (Fig 2e). The CNBD is known to regulate $V_{1/2}$ by exerting a tonic inhibition on the transmembrane pore that is removed by cAMP. Hence the CLP must be in a central position for basal and cAMP-driven control exerted by the CNBD on channel gating. In this context it is worth mentioning that the equivalent mutation of E566K in HCN2 (E515K) has been found in a patient with idiopathic generalized epilepsy[20]. Similarly to that found in HCN4, E515K induces a 30 mV negative shift in the activation curve of HCN2 and a consequent strong reduction of current availability near resting voltages.

The functional significance of the CLP in HCN4 makes this binding site a potential target for the delivery of heart rate control drugs. The high affinity for the CLP shown by Compound 11, which blocks adrenergic stimulation at nanomolar concentrations, proves that it is in principle possible to design an effective drug by *in silico* docking to the CLP. Because of the isoform-specificity of the CLP such drugs may be attractive alternatives to the less isoform-specific channel pore blockers[21].

A most unexpected finding is that prokaryotic and eukaryotic cyclic dinucleotides, are potent antagonist of cAMP in HCN4. The interest in cyclic dinucleotides as second messengers in mammals has so far been restricted to the immune system where they initiate the STING-mediated release of interferon in response to the presence of bacterial[10] or viral[22] DNA in the cytoplasm. Since a number of different cyclic dinucleotides are able to regulate HCN4 activity, we cannot exclude the possibility that other endogenous ligands bind to the CLP. Still it is worth noting that the cyclic-GMP-AMP synthase (cGAS)[23], the key enzyme which

produces the mammalian 2'3'-cGAMP, is abundantly expressed in many different tissues including heart[24]. Other indirect pieces of evidence support a role of cyclic dinucleotides for I_f regulation. For example it has been reported that bacterial endotoxins such as lipopolysaccharides, the major pathogen-associated molecular pattern, cause myocardial depression in sepsis. The bacterial toxins down regulate in a yet unknown fashion the I_f current by inducing a negative shift in the channel activation curve[25-27]. On the basis of present findings and recent data on the immune reaction of mammals showing that cyclic di-nucleotides spread systemically via gap junctions[28], it is reasonable to speculate that the presence of bacteria stimulates an endogenous production of cyclic dinucleotides, which in turn are responsible for the regulation of the I_f current.

Full Methods and any associated references are available in the online version of the paper

Acknowledgments: We thank Xention Ltd, Cambridge, UK, for the generous gift of HCN clones and Christoph Deutscher (BioLog, Bremen) for technical help. This work was supported by SAL-49 Progetto di Cooperazione Scientifica e Tecnologica Regione Lombardia, PRIN (Programmi di Ricerca di Rilevante Interesse Nazionale) 2010CSJX4F and MAE (Ministero Affari Esteri) 01467532013-06-27 to A.M. and by EDICT (European Drug Initiative on Channels and Transporters) to K.S., F. F., C.W.G J., A.M. HCN4 CL-CNBD-(cGMP) atomic coordinates and structure factors have been deposited with the Protein Data Bank with PDB ID code 4KL1. The authors declare no competing financial interests, with the exception of F.S. F.S. is Head of Research & Development of BIOLOG Life Science Institute, which sells cyclic nucleotide analogs for research purposes.

Author Contributions M.L. purified, crystallized, collected, processed and refined X-ray data. M.N. processed and refined X-ray data, prepared some of the Figures and with M.B. revised the manuscript. C.A. prepared the mutants and with M.A. performed the whole-cell experiments on HCN4. S.Z. and I.S. performed the experiments in inside-out. A.B. performed the measurements and with D.D. designed and analyzed the experiments on mouse SAN cells. K.S. performed the docking studies with guidance from A.P.J.

and C.W.G.F. F.S. and D.K. synthesized cyclic dinucleotides and contributed information on their signaling properties. G.T and A.M. designed the study, analyzed data and wrote the paper. M.L. and A.B. equally contributed to this work.

Author Information HCN4 CL-CNBD-(cGMP) atomic coordinates and structure factors have been deposited with the Protein Data Bank with PDB ID code 4KL1. Authors declare no competing financial interests, with the exception of Frank Schwede and Dmitri Kashin. F.S. and D.K. are Head and Staff member, respectively, of Research & Development of BIOLOG Life Science Institute, which sells cyclic nucleotide analogs for research purposes. Correspondence and requests for materials should be addressed to A.M. (anna.moroni@unimi.it).

References

1 DiFrancesco, D. Pacemaker mechanisms in cardiac tissue. *Annu Rev Physiol* **55**, 455-472, doi:10.1146/annurev.ph.55.030193.002323 (1993).

2 Ludwig, A., Zong, X., Jeglitsch, M., Hofmann, F. & Biel, M. A family of hyperpolarization-activated mammalian cation channels. *Nature* **393**, 587-591, doi:10.1038/31255 (1998).

3 Santoro, B. *et al.* Identification of a gene encoding a hyperpolarization-activated pacemaker channel of brain. *Cell* **93**, 717-729 (1998).

4 Zagotta, W. N. *et al.* Structural basis for modulation and agonist specificity of HCN pacemaker channels. *Nature* **425**, 200-205, doi:10.1038/nature01922 (2003).

5 Craven KB, Olivier NB, Zagotta WN. C-terminal movement during gating in cyclic nucleotide-modulated channels. J Biol Chem. 2008 May 23;283(21):14728-38. doi: 10.1074/jbc.M710463200. Epub 2008 Mar 26.

6 Clayton, G. M., Silverman, W. R., Heginbotham, L. & Morais-Cabral, J. H. Structural basis of ligand activation in a cyclic nucleotide regulated potassium channel. *Cell* **119**, 615-627, doi:10.1016/j.cell.2004.10.030 (2004).

7 Schunke, S., Stoldt, M., Novak, K., Kaupp, U. B. & Willbold, D. Solution structure of the Mesorhizobium loti K1 channel cyclic nucleotide-binding domain in complex with cAMP. *EMBO reports* **10**, 729-735, doi:10.1038/embor.2009.68 (2009).

8 Romling, U., Galperin, M. Y. & Gomelsky, M. Cyclic di-GMP: the first 25 years of a universal bacterial second messenger. *Microbiol Mol Biol Rev* **77**, 1-52, doi:10.1128/MMBR.00043-12 (2013).

9 Chen, Z. H. & Schaap, P. The prokaryote messenger c-di-GMP triggers stalk cell differentiation in Dictyostelium. *Nature* **488**, 680-683, doi:10.1038/nature11313 (2012).

10 Wu, J. *et al.* Cyclic GMP-AMP is an endogenous second messenger in innate immune signaling by cytosolic DNA. *Science* **339**, 826-830, doi:10.1126/science.1229963 (2013).

11 Burdette, D. L. *et al.* STING is a direct innate immune sensor of cyclic di-GMP. *Nature* **478**, 515-518, doi:10.1038/nature10429 (2011).

12 DiFrancesco, D. & Tortora, P. Direct activation of cardiac pacemaker channels by intracellular cyclic AMP. *Nature* **351**, 145-147, doi:10.1038/351145a0 (1991).

13 Chandler, N. J. *et al.* Molecular architecture of the human sinus node: insights into the function of the cardiac pacemaker. *Circulation* **119**, 1562-1575, doi:10.1161/CIRCULATIONAHA.108.804369 (2009).

14 Lolicato, M. *et al.* Tetramerization dynamics of C-terminal domain underlies isoform-specific cAMP gating in hyperpolarization-activated cyclic nucleotide-gated channels. *J Biol Chem* **286**, 44811-44820, doi:10.1074/jbc.M111.297606 (2011).

15 Davies, B. W., Bogard, R. W., Young, T. S. & Mekalanos, J. J. Coordinated regulation of accessory genetic elements produces cyclic di-nucleotides for V. cholerae virulence. *Cell* **149**, 358-370, doi:10.1016/j.cell.2012.01.053 (2012).

16 Gao, P. *et al.* Cyclic [G(2',5')pA(3',5')p] Is the Metazoan Second Messenger Produced by DNA-Activated Cyclic GMP-AMP Synthase. *Cell* **153**, 1094-1107, doi:10.1016/j.cell.2013.04.046 (2013).; Diner EJ, Burdette DL, Wilson SC, Monroe KM, Kellenberger CA, Hyodo M, Hayakawa Y, Hammond MC, Vance RE. The innate immune DNA sensor cGAS produces a noncanonical cyclic dinucleotide that activates human STING. Cell Rep. 2013 May 30;3(5):1355-61. doi: 10.1016/j.celrep.2013.05.009. Epub 2013 May 23; Ablasser A, Goldeck M, Cavlar T, Deimling T, Witte G, Röhl I, Hopfner KP, Ludwig J, Hornung V. cGAS produces a 2'-5'-linked cyclic dinucleotide second messenger that activates STING. Nature. 2013 Jun 20;498(7454):380-4. doi: 10.1038/nature12306. Epub 2013 May 30.

17 DiFrancesco, D., Ducouret, P. & Robinson, R. B. Muscarinic modulation of cardiac rate at low acetylcholine concentrations. *Science* **243**, 669-671 (1989).

18 Santoro, B. *et al.* TRIP8b splice variants form a family of auxiliary subunits that regulate gating and trafficking of HCN channels in the brain. *Neuron* **62**, 802-813, doi:10.1016/j.neuron.2009.05.009 (2009).

19 Zolles, G. *et al.* Association with the auxiliary subunit PEX5R/Trip8b controls responsiveness of HCN channels to cAMP and adrenergic stimulation. *Neuron* **62**, 814-825, doi:10.1016/j.neuron.2009.05.008 (2009).

20 DiFrancesco, J. C. *et al.* Recessive loss-of-function mutation in the pacemaker HCN2 channel causing increased neuronal excitability in a patient with idiopathic generalized epilepsy. *The Journal of neuroscience : the official journal of the Society for Neuroscience* **31**, 17327-17337, doi:10.1523/JNEUROSCI.3727-11.2011 (2011).

21 Bucchi, A., Tognati, A., Milanesi, R., Baruscotti, M. & DiFrancesco, D. Properties of ivabradine-induced block of HCN1 and HCN4 pacemaker channels. *J Physiol* **572**, 335-346, doi:10.1113/jphysiol.2005.100776 (2006).

22 Li, X. D. *et al.* Pivotal roles of cGAS-cGAMP signaling in antiviral defense and immune adjuvant effects. *Science* **341**, 1390-1394, doi:10.1126/science.1244040 (2013).

23 Sun, L., Wu, J., Du, F., Chen, X. & Chen, Z. J. Cyclic GMP-AMP synthase is a cytosolic DNA sensor that activates the type I interferon pathway. *Science* **339**, 786-791, doi:10.1126/science.1232458 (2013).

24 Uhlen, M. *et al.* Towards a knowledge-based Human Protein Atlas. *Nat Biotechnol* **28**, 1248-1250, doi:10.1038/nbt1210-1248 (2010).

25 Zorn-Pauly, K. *et al.* Endotoxin impairs the human pacemaker current If. *Shock* **28**, 655-661 (2007).

26 Werdan, K. *et al.* Impaired regulation of cardiac function in sepsis, SIRS, and MODS. *Canadian journal of physiology and pharmacology* **87**, 266-274, doi:10.1139/Y09-012 (2009).

27 Klockner, U. *et al.* Differential reduction of HCN channel activity by various types of lipopolysaccharide. *J Mol Cell Cardiol* **51**, 226-235, doi:DOI 10.1016/j.yjmcc.2011.05.004 (2011).

28 Ablasser, A. *et al.* Cell intrinsic immunity spreads to bystander cells via the intercellular transfer of cGAMP. *Nature*, doi:10.1038/nature12640 (2013).

Figure legends

Figure 1 | Crystal structure of the soluble portion CL-CNBD (C-linker plus CNBD) of HCN4 in complex with cGMP.

a, Ribbon representation of the HCN4 CL-CNBD tetrameric assembly (individual subunits colored in red, green, blue, and magenta). Bound cGMP molecules are shown in stick representation (yellow) surrounded by their electron density ($2F_O$-F_C map contoured at 1σ: cyan mesh). The "canonical" cGMP binding sites and the newly discovered C-linker pocket (CLP) binding sites are indicated. **b,** Ribbon representation of a HCN4 CL-CNBD subunit in complex with cGMP. Helices of the C-linker region and the β-roll are indicated; helices of the C-linker are labeled (A'-C'). **c,** cGMP bound at the HCN4 CLP, showing hydrogen bonds and salt bridges (dashed lines) that stabilize the cGMP molecule. Residues involved in cGMP stabilization are shown in stick representation and labeled (see Supplementary Table 2 for the list of interactions). The HCN4 CL-CNBD subunits are colored accordingly to panel a. **d,** Electrostatic surface at CLP. The blue and red colors highlight positively and negatively charged surfaces, respectively. The bound cGMP is shown as stick representation. **e,** Molecular docking simulation showing a molecule of c-di-GMP bound at the HCN4 CLP.

Residues involved in cGMP stabilization are shown in stick representation and labeled (in red the residues that have been mutated, see Figure 2 for details). **f,** Electrostatic surface at CLP, with the docked c-di-GMP molecule shown as stick representation.

Figure 2 | Effect of c-di-GMP on voltage-dependence of activation of WT and mutant HCN4 channels. **a**, Mean activation curves of HCN4 channels expressed in HEK293T cells and measured in whole-cell, in control (■) and with 100 µM c-di-GMP (Δ). Boltzmann equation fitted to the data points yielded half activation voltage ($V_{1/2}$) values of -98.1 ± 2.7 mV and -96.3 ± 1.7 mV, and slope factor (s) of 8.5 mV and 8.9 mV, respectively for control and c-di-GMP. **b**, Mean activation curves of HCN4 recorded in control (■), 15 µM cAMP (●), 15 µM cAMP + 100 µM c-di-GMP (▲). $V_{1/2}$ values are -99.8 ± 1.5, -79.8 ± 1. 8, -98.1 ± 3 and slope factor (s) 10.3, 9.1, 12 mV for control, cAMP, cAMP + c-di-GMP, respectively. Number of cells in a: ■, n = 3; Δ**,** n = 4; in b: ■, n = 6; ●, n = 6; ▲, n = 5. **c**, Dose-response curve of c-di-GMP, evaluated as recovery from cAMP-induced shift in the activation curve (back shift, mV). The cAMP concentration was 15 µM. Hill equation fitted to the mean data points (n ≥ 3) yielded a $k_{1/2}$ value of 1.8 ± 0.4 µM and n = 1.2 ± 0.2. **d,** Effect of c-di-GMP on HCN4 current measured in inside-out patches. Current recorded at – 140 mV (tails at -40 mV) in control solution (black), 15 µM cAMP (blue) and 15 µM cAMP + 100 µM c-di-GMP (orange). In this experiment the cAMP-induced shift was +15 mV. **Inset**: mean shift (mV) measured in the presence of cAMP (blue, n = 5) and cAMP + 100 µM c-di-GMP (orange, n = 3). **e,** Effect of 100 µM c-di-GMP on channel half activation voltage, $V_{1/2}$, in WT and HCN4 mutants. Data are mean values of n ≥ 3 experiments performed in whole-cell. Control (■), 15 µM cAMP (●), 15 µM cAMP + 100 µM c-di-GMP (▲). **f**, Effect of three different cyclic dinucleotides, c-di-AMP, 3'3'-cGAMP (prokaryotic) and 2'3'cGAMP (eukaryotic), on $V_{1/2}$ (mV) in HCN4 and of c-di-GMP on $V_{1/2}$ (mV) in human HCN2 and HCN1. Control (■), 15 µM cAMP (●), 15 µM cAMP + 100 µM of the indicated cyclic dinucleotide (▲). Number of cells were: c-di-AMP, n = 9, 3'3'-cGAMP, n = 9; 2'3'-cGAMP, n=11, c-di-GMP on HCN2 and HCN1 n = 4.

Figure 3 | Effects of c-di-GMP and 2'3'-cGAMP on voltage dependence of I_f activation and spontaneous rate in SAN.

a, Representative whole-cell I_f currents recorded in control and in the presence of either 100 µM c-di-GMP or 100 µM 2'3-cGAMP, at the indicated voltages, without (top) and with 10 µM cAMP in the pipette (bottom). **b, c**, Mean I_f activation curves measured in the absence (filled symbols) and in the presence of 10 µM cAMP (open symbols) in control (circles) and with 100 µM c-di-GMP (b, squares) or 100 µM 2'3'-cGAMP (c, diamonds) in the pipette. Comparison of data in b and in c always involves day-matched preparations. Number of cells in b: ●, n = 9; ○, n = 8; ■, n = 8; □, n =13; in C: ●, n =5;○, n = 4; ♦, n = 6; ◊, n =6. **d**, Left, representative recordings of single SAN cell spontaneous activity in control and in the presence of 2'3'-cGAMP (100 µM). Right, mean spontaneous rate recorded in control and in the presence of 2'3'-cGAMP. * P< 0.05, Student t-test.

Figure 4 | Effect of C11 on HCN4, I_f channels and spontaneous rate in SAN.

a, Exemplary screening procedure for active compounds performed in HEK293T cells in whole cell. A mixture of three compounds selected by docking (mix), inhibits the cAMP-induced positive shift in HCN4 activation curve. Individual testing of the three molecules shows that C11 (but not C5 and C8) is the active molecule as it reproduces the effect of the mix. **b**, Effect of 100 µM C11 on the activation curve of HCN4. Control (■), 15 µM cAMP (●), 15 µM cAMP +100 µM C11 (▲). Number of cells: ■, n = 4; ●, n = 5; ▲, n = 4. Boltzmann fit yielded $V_{1/2}$ values of -94.8 ± 1.9, -79.3 ± 1.7, -94.2 ± 2.7 and slope factor (s) = 9.6, 10.7, 12.2 mV for control, cAMP, cAMP + C11, respectively. **c**, Dose-response curve of C11 evaluated as recovery of the shift induced by cAMP in HCN4 (back shift, mV). Data is mean values of n ≥ 3. Fitting of Hill equation to the experimental data yielded a $k_{1/2}$ value of 0.42 ± 0.1 µM and n = 0.8 ± 0.1 **d,** Electrostatic surface at CLP, with inhibitor C11 docked using eHiTS. **e,** Docking of C11 bound in the CLP of HCN4 as predicted using eHiTS. Residues involved in the predicted binding pose are shown in stick representation and labeled (for clarity, the orientation of the CLP is identical to that in panels c-f of Fig. 1). **f**, Effect of 100 µM

C11 on channel half activation voltage, $V_{1/2}$ (mV), in HCN4 WT and in the HCN4 mutants F613T and Y682F. Effect of 200 µM C11 on $V_{1/2}$ (mV) in HCN2. Data is mean values of n ≥ 3 experiments performed in whole cell. Control (■), 15 µM cAMP (●), 15 µM cAMP + 100 µM (or 200 µM) C11 (▲). **g**, Representative whole-cell I_f currents recorded in control and in the presence of 100 µM C11, at the indicated voltages, without (top) and with 10 µM cAMP in the pipette (bottom). **h**, Mean I_f activation curves measured in the absence (filled symbols) and in the presence of 10 µM cAMP (open symbols) in control (circles) and with 100 µM C11(triangles) in the pipette. Comparison of data in **h** always involves day-matched preparations. Number of cells in **h**: ●, n =15;○, n = 9; ▲, n = 15; Δ, n = 7. **i**, Left, representative recordings of single SAN cell spontaneous activity in control and in the presence of C11 (100 µM). Right, mean spontaneous rate recorded in control and in the presence of C11. * P< 0.05, Student t-test.

Supplementary materials

Material and Methods

Supplementary Tables 1 to 3

Supplementary Figs 1 to 5

References (29-43)

Material and Methods

Protein preparation

The cDNA fragment comprising the C-linker (CL) and CNBD region of human HCN4 (residues 521-723), was cloned into a modified pET-24b plasmid, transformed into *E. coli* Rosetta strain, overexpressed and purified as previously described[14].

Crystallization and structure determination

Crystallization trials were set up in 96-well sitting drop plates (Greiner) using the Orxy 8.0 crystallization robot (Douglas Instruments) and stored at 4 °C. Crystallization conditions were eventually further optimized manually in 24-well hanging-drop plates. Crystals of the HCN4 CL-CNBD-(cGMP) complex (protein concentration 7-13 mg/ml, 2.5-50 mM cGMP) were grown by vapor-diffusion method using 10-15% PEG3350, 200 mM sodium acetate buffer (pH 5.0) and 200 mM ammonium phosphate as a precipitant solution. Crystals were cryoprotected with the same solution with a 5% increase of PEG3350 and with the addition of 25% glycerol. A full data set was collected at 100K to 2.7 Å resolution, using synchrotron radiation (λ= 0.97238 A, ID29 beamline, ESRF, Grenoble, France). Raw data were processed with Mosflm[29] and Scala[30] and the structure was solved by molecular replacement using the program MolRep[31] for the HCN4 CL-CNBD-(cGMP) complex. The crystal structure of human HCN4 in complex with cAMP[14] (PDB entry-code 3U11) was used as search model. To avoid model bias, the bound cAMP was removed from the search model. Several cycles of manual rebuilding, using the program COOT[32], and refinement, using the program REFMAC5[33] (rigid body and restrained refinement), were carried out to improve the electron density map. The final R-factor and R-free are 21.1 % and 27.2 %, respectively. The program Procheck[34] was used to assess protein stereochemical quality (Ramachandran statistics: allowed region = 92.7%, favorably allowed region = 7.3%). The program PISA[35] was used to identify and analyze the quaternary assemblies.

Constructs

The *hHCN4* and *hHCN2* complementary DNA was inserted in the eukaryotic expression vector pcDNA 3.1 (Clontech Laboratories). Mutations were generated by site-directed mutagenesis (QuikChange site-directed mutagenesis kit; Agilent Technologies) and confirmed by sequencing.

Electrophysiology of HEK293T cells

Complementary DNA of wild-type and mutant channels was co-transfected for transient expression into HEK293T cells with a plasmid containing green fluorescent protein. One to five days after transfection, GFP-expressing cells were selected for patch-clamp experiments at room temperature (25 to 26 °C) either in whole-cell configuration or inside-out by means of macropatch. The pipettes used in whole-cell experiment contained (mM): 10 NaCl, 130 KCl, 1 egtazic acid (EGTA), 0.5 $MgCl_2$, 2 ATP (Na salt) and 5 HEPES–KOH

buffer (pH 7.2). The extracellular baths solution in whole-cell experiments contained (mM): 110 NaCl, 30 KCl, 1.8 $CaCl_2$, 0.5 $MgCl_2$, 1 $BaCl_2$, 2 $MnCl_2$ and 5 HEPES–NaOH buffer (pH 7.4). The pipettes used in the inside-out macropatch experiments contained (mM): 70 NaCl, 70 KCl, 1.8 $CaCl_2$, 1 $MgCl_2$, and 5 HEPES–KOH buffer (pH 7.4); a solution containing (mM) 144 KCl, 1 NaCl, 1 EGTA, 1 $MgCl_2$ and 10 HEPES–KOH buffer (pH 7.2) perfused the intracellular sides of the patches. Because the midpoint of activation of HCN4 shifted by approximately 40 mV in a hyperpolarized direction after patch excision, we waited at least 5 min after obtaining inside-out patches before beginning experiments. In most cases, this was sufficient to limit drift to a few millivolts over the time course of the experiment. cAMP, c-di-GMP, c-di-AMP, 2'3'-cGAMP and 3'3'-cGAMP (BioLog Life Science Institute, Bremen, Germany) and compound 11 (Peakdale Molecular, Chapel-en-le-Frith, UK) were added at the indicated concentrations to the pipette's solution in whole-cell or to the bath solution in inside-out. All values are given as mean ± SEM.

Data analysis

The activation curves for *h*HCN4 and *h*HCN2 currents recorded in HEK293T cells under whole-cell conditions were obtained by standard activation and deactivation protocols and analyzed by the Boltzmann equation, $y=1\div\{1+\exp[(V-V_{1/2})\div s]\}$, where y is fractional activation, V is voltage, $V_{1/2}$ half-activation voltage, and s the inverse slope factor (mV). Mean activation curves were obtained by fitting individual curves from each cell to the Boltzmann equation and averaging half-activation voltages and inverse slope factors. Shifts of the voltage–dependent activation induced by perfusing cyclic nucleotides on the intracellular side of macropatches were evaluated by measurement of the change in holding potential producing superimposition of current traces in control and in the presence of cGMP according to a previously developed protocol[36]. The activation curves in inside-out macropatches and the shifts induced by cGMP were obtained by slow voltage ramp protocols and calculated as previously reported[37]. The dose–response curves were analyzed by the Hill equation, as follows: $S\div S_{max} = 1\div [1+(k_{1/2}\div[\text{ligand}])^n]$, where S is the shift (cAMP or cGMP) or the back shift (for cyclic dinucleotides or C11), $k_{1/2}$ is the half-maximal concentration, and *n* is the Hill factor. In inside-out measurements, each patch was exposed to the ligand only once. All values are given as mean ± SEM.

Isolation and electrophysiology of sinoatrial node cells

Animal protocols conformed to the guidelines of the care and use of laboratory animals established by Italian (DL. 116/1992) and European (86/609/CEE) directives. 2-6 month old C57/Bl6 mice were deeply anaesthetized by isofluoran and euthanized by cervical dislocation. Single SAN myocytes were obtained as described previously[38]. Isolated cells were maintained at 4 °C in Tyrode solution (in mM: 140 NaCl, 5.4 KCl, 1.8 $CaCl_2$, 1 $MgCl_2$, 5.5 D-glucose, 5 HEPES-NaOH (pH 7.4) for the day of the experiment and patch-clamped in the whole-cell configuration at 35±0.5 °C. The pipette solution contained (in mM): 10 NaCl, 130 KCl, 1 egtazic acid (EGTA), 0.5 $MgCl_2$, 2 ATP (Na salt) and 5 HEPES–KOH buffer (pH 7.2). When indicated cAMP (10 μM), c-di-GMP (100 μM), and compound 11 (100 μM) were added to the pipette's solution. The I_f current was recorded from single cells superfused with Tyrode solution to which $BaCl_2$ (1 mM), and $MnCl_2$ (2 mM) were added to improve I_f dissection.

I_f activation curves were obtained using a two voltage step protocol in which test voltage steps were applied from a holding potential of -35 mV to the range -35/-135 mV (20 mV interval). Test steps had variable duration so as to reach steady-state activation at all voltages and were followed by a step to -125 mV. Plots of normalized current amplitudes measured at -125 mV as a function of test voltage were fitted with the Boltzmann (see above). Spontaneous activity was recorded from single SAN cells in Tyrode solution and the rate was measured with customized software as described previously[39]. Data was acquired at 1 kHz using an Axopatch 200B amplifier and pClamp10.2 (Molecular Devices, Sunnyvale CA). Data was analyzed off-line using Clampfit 10.2 (Molecular Devices) and Origin 8.5 (OriginLab Corp., Northampton MA). Statistical differences were determined at the $P < 0.05$ level by either ANOVA or Student's t-test. All values are given as mean ± SEM.

Western blot

Fifty-percent confluent HEK293TT cells were transfected (in 35 mm diameter wells) respectively with hHCN4 (2ug) and hSTING (2ug) with Lipofectamine2000 reagent (Invitrogen). pMAX-GFP plasmid was co-transfected. Expression of hHCN4 was verified by patch-clamp recordings. After 48hrs, cells were resuspended in PBS pH7.4 supplemented with Triton X-100 1%(v/v) and protease inhibitors cocktail

(Complete, Roche). Cells were gently broken with a 27G needle. Cells debris was centrifuged at 8000 xg for 10 minutes at 4°C. The supernatant was collected and analyzed by SDS-PAGE and western blot. For immunodetection STING antibody (Cell Signaling Technology) and anti-rabbit HRP conjugated were used.

Virtual high-throughput screening using eHiTS

The electronic high-throughput screening program eHiTS[40,41] utilizes an exhaustive systematic search algorithm that considers all docking poses that avoid severe steric clashes with the protein. The system employs unique graph matching algorithms and dock tables which are stored in SQL databases. In the first instance, the binding pocket is defined by a steric grid which divides regions into separate pockets and identifying all possible interaction sites. The ligand is divided into rigid fragments and connecting flexible chains. Each fragment is wrapped into a polyhedron shape with chemical properties assigned to the vertices of the polyhedron. All rigid fragments are docked to every possible place in the newly identified binding site and scored for predicted binding affinity. Initially, a simple and fast chemical flag based statistical scoring function is used during the rigid fragment-docking and pose-matching phases. Using eHiTS (version 9.0), a library containing 12000 compounds from Peakdale Molecular (http://www.peakdale.co.uk) was screened against the X-ray crystal structure of HCN4. 1000 compounds were selected for evaluation using the *de novo* design program SPROUT [42]. From this set, 11 molecules were selected for purchase based upon their predicted binding affinity to the protein.

Supplementary Figure 1 | Alignment of HCNs sequences

Alignment of the C-linker (A'-F' helices) + CNBD (helices A, P, B, C, beta strands 1-8) sequences of human HCN1, HCN2 and HCN4 (NCBI Reference Sequence: NP_066550.2, NP_001185.3, NP_005468.1, respectively). The orange line marks the residues surrounding the newly identified C linker pocket (CLP). The amino acids interacting with the cGMP molecule found in the CLP (PDB ID code 4KL1) are highlighted in orange. In red are the amino acids different in the three isoforms.

Supplementary Figure 2 | Comparison of HCNs isoforms

a, Overall structural comparison of CL-CNBDs in complex with cGMP from HCN4 (green), and HCN2 (grey, PDB entry-code 1Q3E)[4]. The comparison has been made by superimposing the CNBD core domain of the HCN isoforms. For clarity only the Cα backbones at the C-linker regions are shown. The rms deviation for residues at the C-linker regions ranges between 1.1 Å and 1.4 Å depending on the subunits present in the crystal asymmetric units. **b**, Overall structural comparison (similar to panel **a**) of CL-CNBDs in complex with cAMP from HCN4 (blue; PDB entry-code 3U11), HCN1 (yellow; PDB entry-code 3U0Z), and HCN2 (orange; PDB entry-code 3U10)[14]. The Cα backbones of the HCN1 and HCN2 cluster together (rms deviation of 1.4 Å for residues at the C-linker regions for all subunits present in the crystal asymmetric units), whereas differences are evident, especially for the C' and D'-helices, for the HCN4 isoform (rms deviation for residues at the C-linker regions ranging between 1.6 Å and 1.7 Å for HCN4 and HCN1 and between 2.5 Å and 2.6 Å for HCN4 and HCN2, depending on the subunits present in the crystal asymmetric units). Helices at the C-linker region are indicated, together with the position of the cGMP binding site at the C-linker pocket of HCN4. **c**, Close up view of the canonical cGMP binding pocket in the CNBD of HCN4 (green) reveals a perfect agreement of the cGMP binding mode with the HCN2 structure (grey) co-crystallized with cGMP (PDB: 1Q3E)[4]. As in HCN2, the cGMP molecule is found in the *syn* configuration, bound between the beta roll and the C helix. All the agonist-protein interactions found in HCN2 are conserved (Supplementary Table 2b), including the purine-specific hydrogen bonds with Thr670 of the beta-roll and with Arg710 of the C helix. Alpha helices and beta sheets of the CNBD are labeled.

Supplementary Figure 3 | Effect of cGMP on HCN4 in HEK293T cells

a, Exemplary activation curve of HCN4 channels measured in Control (■) and 1 mM cGMP (●), from an inside-out macropatch. Boltzmann fit yielded $V_{1/2}$ of -120 mV and -108 mV and s of 8 mV and 7 mV for

control and cGMP respectively. **Inset**: current recorded from the same macropatch during a two-step protocol from a holding potential of -30 mV to -130 mV and to -60 mV, before (black) and after (red) the addition of 1 mM cGMP **b**, Mean cGMP-dependent shifts (in mV) measured as a function of increasing cGMP concentration. Each data point is the average of three to nine patches. Fitting of the data with the Hill equation yields values of 13.2 μM for the half maximal cGMP concentration ($k_{1/2}$) and 0.72 for the Hill coefficient *n*. **c**, Effect of high concentrations of cGMP (5 and 10 mM). HCN4 current recorded in inside-out macropatch at the test voltage of -110 mV, in control solution (black) and after the addition of 5 mM (red) or 10 mM cGMP (blue). cGMP shifted $V_{1/2}$ by 13 mV (evaluated by changing the holding potential, see Methods); **d**, Effect of cGMP in the presence of high concentrations of cAMP on HCN4. Current recorded at the test voltage of -110 mV in control (black) and after the addition of 5 mM cAMP (red), 5 mM cAMP + 1mM cGMP (blue) and 5 mM cAMP + 2.5 mM cGMP (green). Such a high cAMP concentration prevents competition with cGMP for the canonical binding pocket in the CNBD. In HCN4, cAMP binds with a $k_{1/2}$ of 1.5 μM[43], an order of magnitude higher than that measured for cGMP (panel b).

Supplementary Figure 4 | Chemical structures of c-dinucleotides and Compound 11

Structures of C-linker pocket binders c-di-GMP, c-di-AMP, two linkage isomers of cyclic GMP-AMP, the bacterial 3'3'-cGAMP, and the eukaryotic 2'3'-cGAMP and the chemically unrelated compound 11 ((N'-biphenyl-2-yl-N-[1-(3-cyanobenzyl)piperidin-4-yl]-N-(pyridin-3-ylmethyl)urea).

Supplementary Figure 5 | HCN4 currents recorded with c-di-GMP in whole-cell and in inside–out.

a, b, Representative whole-cell currents from HEK293T cells expressing HCN4 channels recorded at the indicated voltages in control and in the presence of c-di-GMP, without (a) and with (b) 15 μM cAMP in the pipette. **c**, HCN4 currents recorded in one inside-out macropatch at –140 mV (tails at -40 mV) in control

solution (black), 15 µM cAMP (red), 15 µM cAMP + 100 µM c-di-GMP (green) and 1 mM cAMP + 100 µM c-di-GMP (blue). The cAMP-induced shift was +15 mV (measured by changing the holding potential, see Methods). **d**, activation curve of HCN4 channels measured in one inside-out macropatch by slow voltage ramps[35] in 100 µM c-di-GMP without (black) and with (red) 1 mM cAMP. In the presence of c-di-GMP, 1 mM cAMP does not induce the positive shift in the channel activation curve. Fitting of Boltzmann curve yielded $V_{1/2}$ = -141.5 mV, s = 10.1.

Supplementary Figure 6 | The effect of c-di-GMP on HCN4 is not mediated by the activation of STING and is not cAMP-specific. a, STING is not detectable in HEK293T cells. Western blot analysis of extracts from HEK293T cells, untransfected (UN), transfected with a cDNA expression construct encoding hHCN4 (HCN4) or transfected with a cDNA expression construct encoding hSTING (STING). Immunodetection has been done with the STING antibody. **b**, Effect of c-di-GMP in the presence of cGMP. The measurement was performed in whole cell, in HEK293T cells expressing HCN4. Boltzmann equation fitted to the data point yielded the following values for half activation voltage ($V_{1/2}$) and slope factor (s): control (■), -103.8 ± 0.14 mV and 11.8 ± 0.13 mV, (n =3); + 1 mM cGMP (●), -91.2 ± 0.13 mV and 8.36 ± 0.12 mV, (n =3); 1 mM cGMP + 100 uM c-di-GMP (▲), -105 ± 0.25 mV and 14.2 ± 0.23 mV, (n =3).

Supplementary Figure 7 | Effect of c-di-AMP, 3'3'-cGAMP and 2'3'cGAMP on the voltage dependence of HCN4 activation.

Mean activation curves of HCN4 channels expressed in HEK293T cells and recorded in whole cell configuration in the absence (black squares) and in the presence of 15 µM cAMP (blue circle). Cyclic nucleotides were added 100 µM in the presence of 15 µM cAMP (orange triangle). Boltzmann equations were fitted to the mean data points (n≥3) and the resulting $V_{1/2}$ and s were: c-di-AMP, ■, -97.1 ± 0.2 mV, 10

mV; ●, -82.7 ± 0.2 mV, 11 mV; ▲, -96.3 ± 0.3 mV, 12 mV; 3'3'-cGAMP, ■, -96.5 ± 0.3 mV, 9.1 mV; ●, -82 ± 1.5 mV, 9.7 mV; ▲, -97.4 ± 0.12 mV, 7.7 mV: 2'3'cGAMP, ■, -96.8 ± 0.5 mV, 9.3 mV; ●, -79.3 ± 2.2 mV, 10.4 mV; ▲, -96.5 ± 0.8 mV, 12.3 mV.

Supplementary Figure 8 | Characterization of the interaction of mammalian 2'3'cGAMP with HCN4

a, Molecular docking simulation showing a molecule of 2'3'-cGAMP bound at the HCN4 CLP. Residues involved in 2'3'-cGAMP stabilization are shown in stick representation and labeled. **b,** Dose-response curve of the effect of 2'3'-cGAMP on HCN4. The effect was evaluated as inhibition of the cAMP-induced shift (back shift) in the voltage-dependent activation of HCN4. Measurements were performed in the whole cell configuration in HEK293T cells expressing HCN4. The pipette solution contained 15 μM cAMP and the indicated 2'3'cGAMP concentrations. Solid line represent fitting of Hill equation to data, yielding the following values for $k_{1/2}$ = 116 nM and n = 0.95. Number of cells varied between 3 and 15.

Supplementary references

Structure of Human cGAS Reveals a Conserved Family of Second-Messenger Enzymes in Innate Immunity ⍰⍰Philip J. Kranzusch, Amy Si-Ying Lee, James M. Berger, Jennifer A. Doudna Cell Reports - 30 May 2013 (Vol. 3, Issue 5, pp. 1362-1368)

29 Leslie, A.G.M. *MOSFLM User Guide, Mosflm Version 6.2.3.*, MRC laboratory of Molecular Biology, Cambridge, UK (2003).

30 Evans, P. Scaling and assessment of data quality. *Acta Crystallogr D Biol Crystallogr* **62**, 72-82, doi:10.1107/S0907444905036693 (2006).

31 Vagin, A. & Teplyakov, A. MOLREP: an automated program for molecular replacement. *Journal of Applied Crystallography* **30**, 1022-1025, doi:Doi 10.1107/S0021889897006766 (1997).

32 Emsley, P. & Cowtan, K. Coot: model-building tools for molecular graphics. *Acta Crystallogr D Biol Crystallogr* **60**, 2126-2132, doi:10.1107/S0907444904019158 (2004).

33 Murshudov, G. N., Vagin, A. A. & Dodson, E. J. Refinement of macromolecular structures by the maximum-likelihood method. *Acta Crystallogr D Biol Crystallogr* **53**, 240-255, doi:10.1107/S0907444996012255 (1997).

34 Laskowski, R. A., Macarthur, M. W., Moss, D. S. & Thornton, J. M. Procheck - a Program to Check the Stereochemical Quality of Protein Structures. *Journal of Applied Crystallography* **26**, 283-291, doi:Doi 10.1107/S0021889892009944 (1993).

35 Krissinel, E. & Henrick, K. Detection of protein assemblies in crystals. *Computational Life Sciences, Proceedings* **3695**, 163-174 (2005).

36 Accili, E. A. & DiFrancesco, D. Inhibition of the hyperpolarization-activated current (if) of rabbit SA node myocytes by niflumic acid. *Pflugers Arch* **431**, 757-762 (1996).

37 DiFrancesco, D. & Mangoni, M. Modulation of single hyperpolarization-activated channels (i(f)) by cAMP in the rabbit sino-atrial node. *J Physiol* **474**, 473-482 (1994).

38 Baruscotti, M. *et al.* Deep bradycardia and heart block caused by inducible cardiac-specific knockout of the pacemaker channel gene Hcn4. *Proc Natl Acad Sci U S A* **108**, 1705-1710, doi:10.1073/pnas.1010122108 (2011).

39 Bucchi, A., Baruscotti, M., Robinson, R. B. & DiFrancesco, D. I(f)-dependent modulation of pacemaker rate mediated by cAMP in the presence of ryanodine in rabbit sino-atrial node cells. *J Mol Cell Cardiol* **35**, 905-913 (2003).

40 Zsoldos, Z., Reid, D., Simon, A., Sadjad, B. S. & Johnson, A. P. eHiTS: an innovative approach to the docking and scoring function problems. *Curr Protein Pept Sci* **7**, 421-435 (2006).

41 Zsoldos, Z., Reid, D., Simon, A., Sadjad, S. B. & Johnson, A. P. eHiTS: a new fast, exhaustive flexible ligand docking system. *J Mol Graph Model* **26**, 198-212, doi:10.1016/j.jmgm.2006.06.002 (2007).

42 Zsoldos, Z., Szabo, I., Szabo, Z. & Johnson, A. P. Software tools for structure based rational drug design. *Journal of Molecular Structure-Theochem* **666**, 659-665, doi:DOI 10.1016/j.theochem.2003.08.105 (2003).

43 Milanesi, R., Baruscotti, M., Gnecchi-Ruscone, T. & DiFrancesco, D. Familial sinus bradycardia associated with a mutation in the cardiac pacemaker channel. *N Engl J Med* **354**, 151-157, doi:10.1056/NEJMoa052475 (2006).

Figure 1

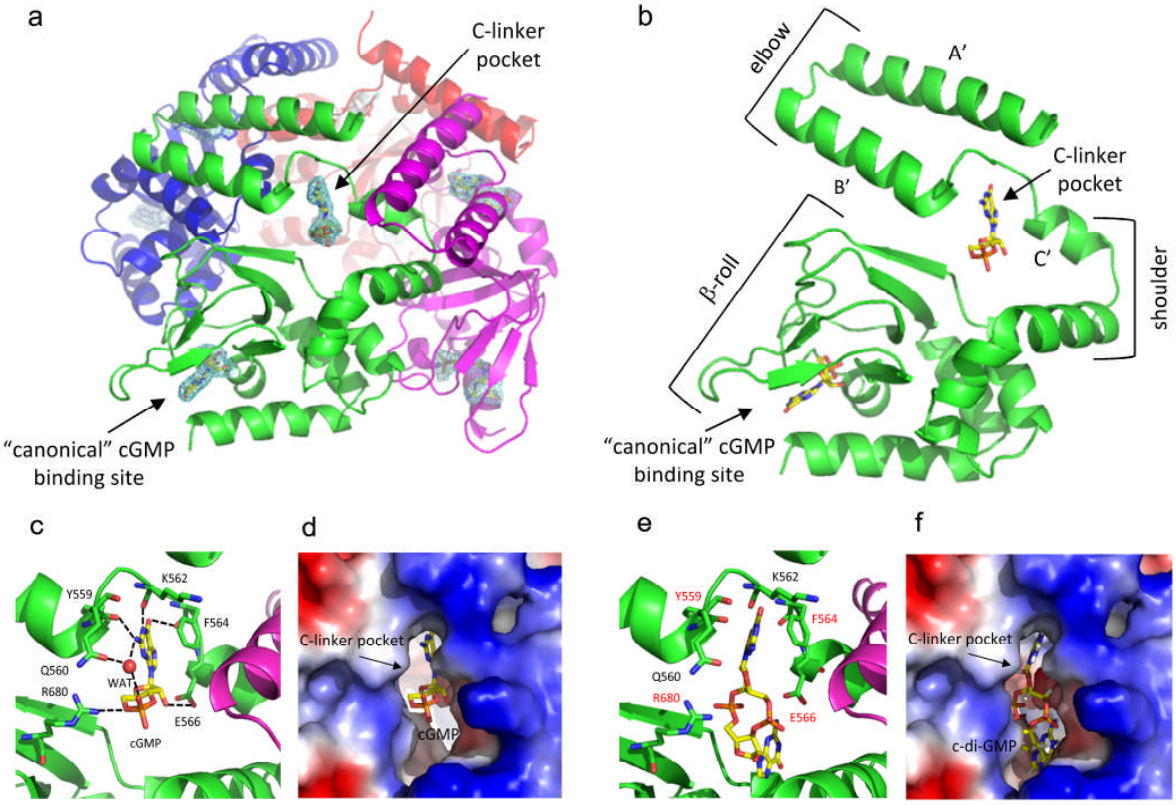
a
C-linker pocket
"canonical" cGMP binding site
b
elbow
A′
C-linker pocket
B′
β-roll
C′
shoulder
"canonical" cGMP binding site
c
Y559
K562
F564
Q560
WAT
R680
E566
cGMP
d
C-linker pocket
cGMP
e
Y559
K562
F564
Q560
R680
E566
f
C-linker pocket
c-di-GMP

Figure 2

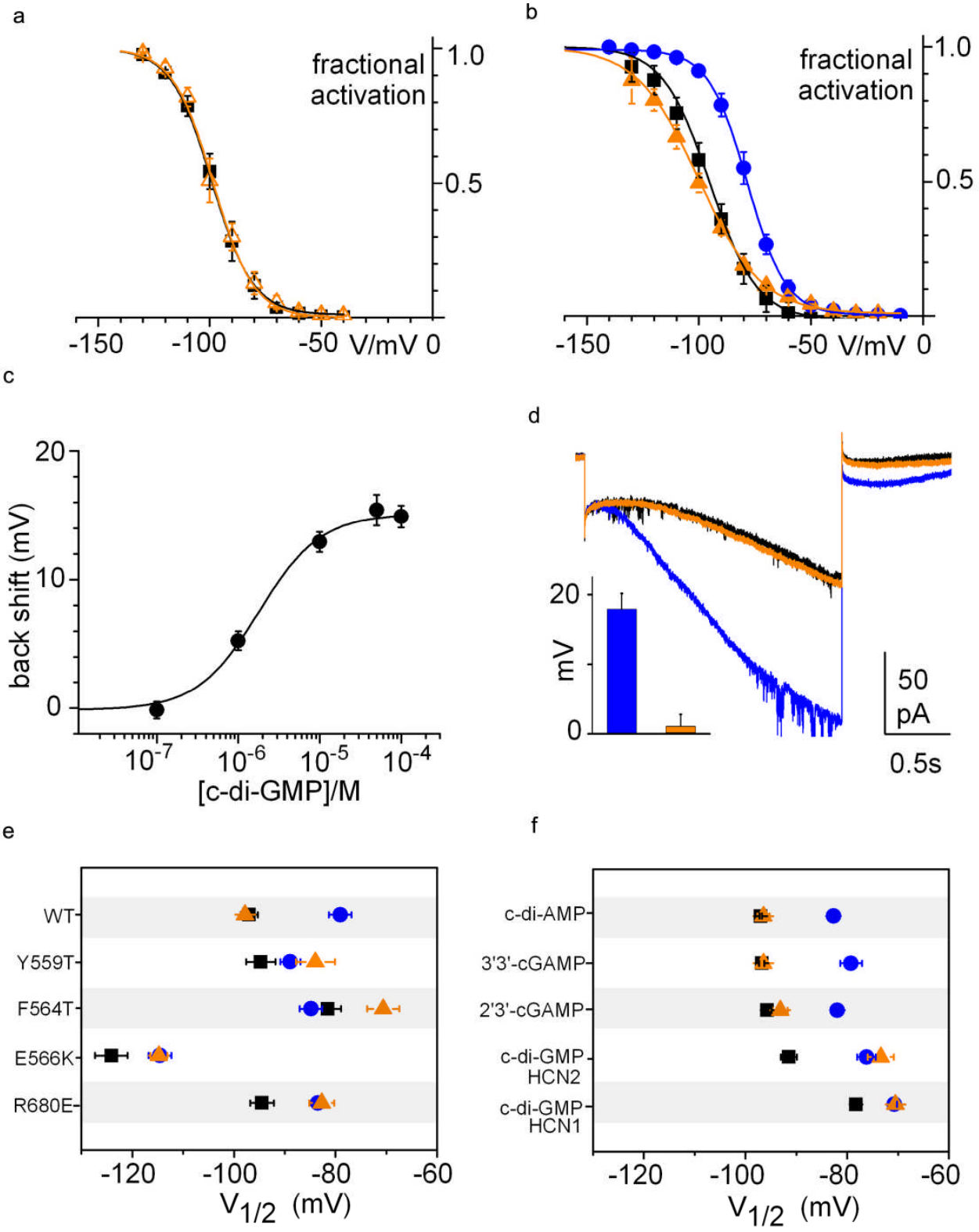
a
fractional activation
1.0
0.5
-150
-100
-50
V/mV
0
b
fractional activation
1.0
0.5
-150
-100
-50
V/mV
0
c
back shift (mV)
20
10
0
10^{-7}
10^{-6}
10^{-5}
10^{-4}
[c-di-GMP]/M
d
20
mV
0
50
pA
0.5s
e
WT
Y559T
F564T
E566K
R680E
-120
-100
-80
-60
$V_{1/2}$ (mV)
f
c-di-AMP
3'3'-cGAMP
2'3'-cGAMP
c-di-GMP HCN2
c-di-GMP HCN1
-120
-100
-80
-60
$V_{1/2}$ (mV)

Figure 3

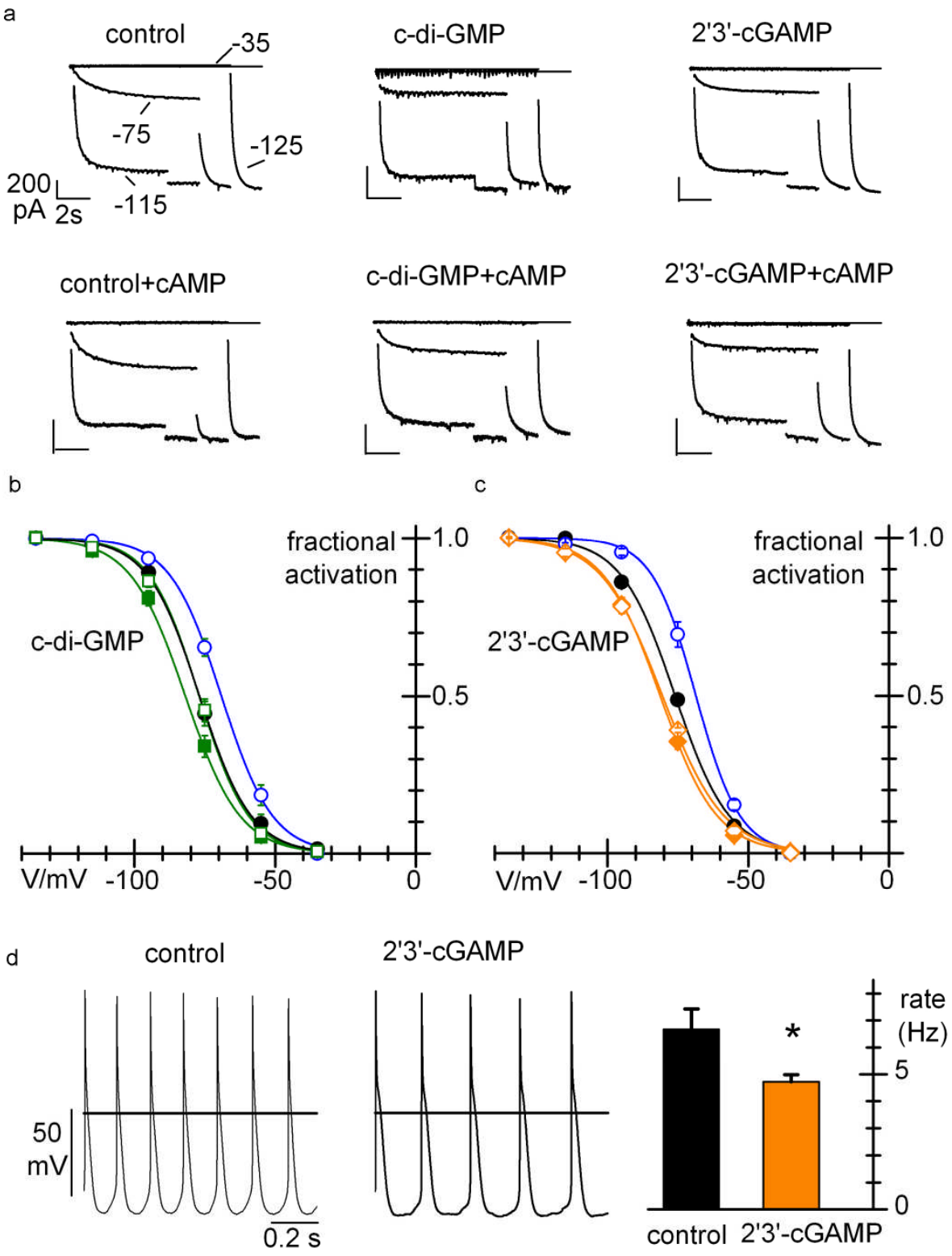
a
control
-35
-75
-125
-115
200 pA
2s
c-di-GMP
2'3'-cGAMP
control+cAMP
c-di-GMP+cAMP
2'3'-cGAMP+cAMP
b
c
fractional activation
1.0
0.5
c-di-GMP
V/mV -100 -50 0
fractional activation
1.0
0.5
2'3'-cGAMP
V/mV -100 -50 0
d
control
2'3'-cGAMP
50 mV
0.2 s
*
rate (Hz)
5
0
control
2'3'-cGAMP

Figure 4

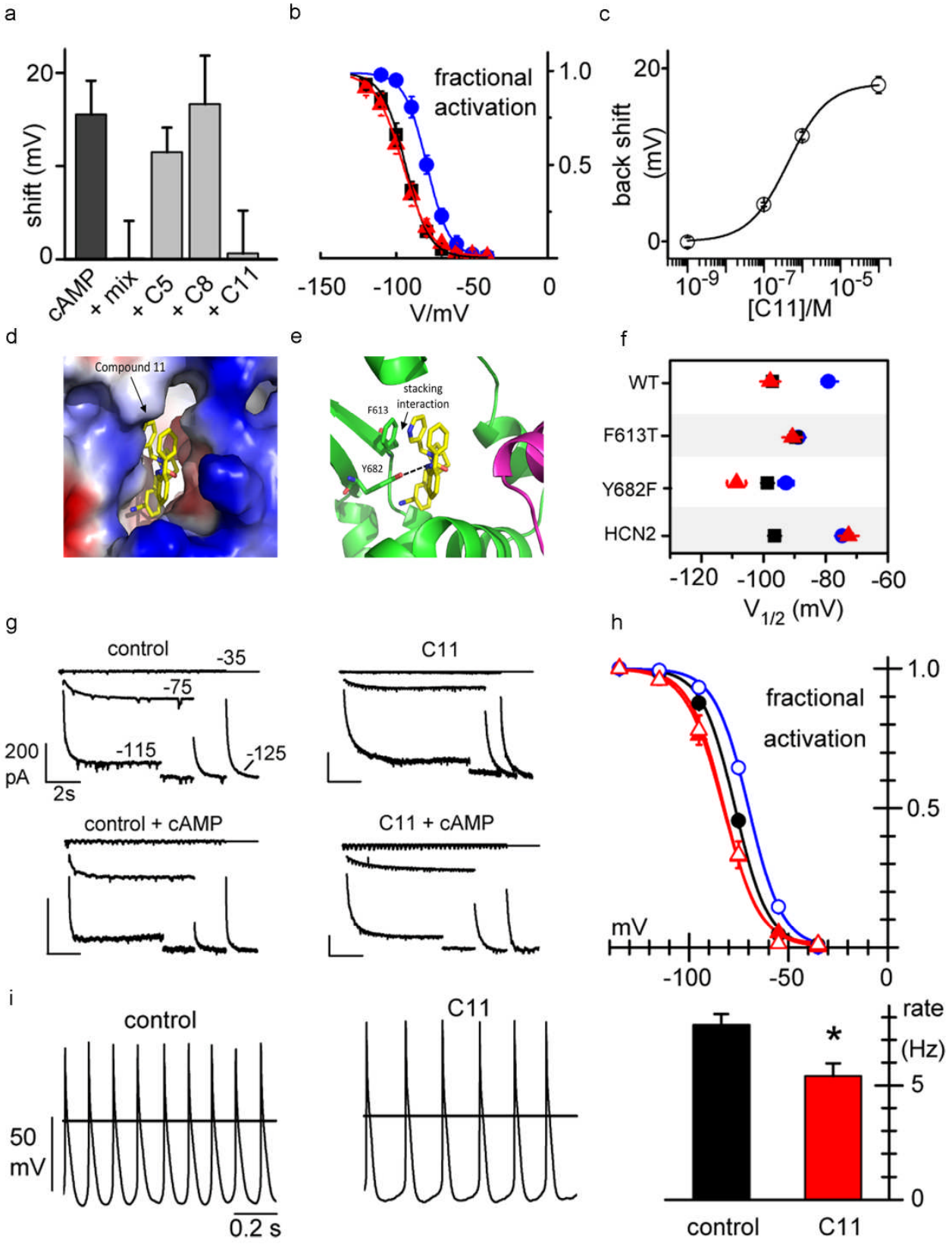
a
shift (mV)
20
0
cAMP
+ mix
+ C5
+ C8
+ C11
b
fractional activation
1.0
0.5
-150
-100
-50
0
V/mV
c
back shift (mV)
20
0
10-9
10-7
10-5
[C11]/M
d
Compound 11
e
stacking interaction
F613
Y682
f
WT
F613T
Y682F
HCN2
-120
-100
-80
-60
V1/2 (mV)
g
control
-35
-75
-115
-125
200 pA
2s
C11
control + cAMP
C11 + cAMP
h
fractional activation
1.0
0.5
mV
-100
-50
0
i
control
C11
50 mV
0.2 s
rate (Hz)
5
0
*
control
C11

Supplementary Table 1 | Data collection and refinement statistics of HCN4 C-linker + CNBD In complex with cGMP

	HCN4 cGMP
Data collection	
Space group	$P2_12_12_1$
Cell dimensions	
a, *b*, *c* (Å)	97.1, 99.0, 109.6
α, β, γ (°)	90.0, 90.0, 90.0
Resolution (Å)	58.62-2.70 (2.85-2.70) *
R_{sym} or R_{merge}	0.10 (0.45)
$I / \sigma I$	18.1 (4.3)
Completeness (%)	100 (100)
Redundancy	7.1 (7.3)
Refinement	
Resolution (Å)	2.7
No. reflections	26671
R_{work} / R_{free}	21.1/ 27.2
No. atoms	6815
Protein	6484
Ligand/ion	212
Water	118
B-factors	
Protein	34.3 (A)¶, 37.9 (B), 33.7 (C), 44.2 (D)
cGMP (canonical binding site)	17.6 (A), 25.1 (B), 25.7 (C), 30.9 (D)
cGMP (C-linker binding site)#	57.0 (A), 64.3 (B), 63.7 (C), 84.8 (D)
Water	31.5
R.m.s. deviations	
Bond lengths (Å)	0.023
Bond angles (°)	1.9

*Highest-resolution shell is shown in parentheses.
¶ Subunit chain in the crystal asymmetric unit
# The cGMP occupancy at the C-linker binding site is 1.0 for the A and C chains and 0.7 for the B and D chains.

Supplementary Table 2| Protein-cGMP interactions

a, HCN4 chain A-cGMP interactions in the C-linker pocket (CLP). Polar contacts (<3.5 A) are reported in detail.

Atom type (HCN4)	Atom type (cGMP)	HCN4 residues
O	N2	Tyr559
O	N2	Lys562
O	N1	Lys562
N	O6	Phe564
O	O6	Phe564
OE2	O2'	Glu566
NH2	O5'	Arg680

b, HCN4-cGMP interactions in the canonical binding pocket in the CNBD. Polar contacts (<3.5 A) are reported in detail. Contacts conserved between the crystal structure of HCN2 (1Q3E)[4] and the four chains (**4KL1** A-D) are shown in the same line.

Atom type (HCN4)	Atom type (cGMP)	HCN2 (1Q3E)	HCN4 residues			
		1Q3E	**4KL1 A**	**4KL1 B**	**4KL1 C**	**4KL1 D**
N	O2'	Gly581	Gly659	Gly659	Gly659	Gly659
OE2	O2'	Glu582	Glu660	Glu660	Glu660	Glu660
O	O3'					Ile661
N	O2A	Cys584	Cys662	Cys662	Cys662	Cys662
NH1	O2A	Arg591	Arg 669	Arg 669	Arg 669	Arg 669
N	O1A	Thr592	Thr 670	Thr 670	Thr 670	Thr 670
OG1	O1A	Thr 592	Thr 670	Thr 670	Thr 670	Thr 670
OG1	N2	Thr 592	Thr 670	Thr 670	Thr 670	Thr 670
O	N1	Arg 632	Arg 710	Arg 710	Arg 710	Arg 710
NH1	O2'	Arg 632	Arg 710	Arg 710	Arg 710	Arg 710
O	O6				Arg 713	

Supplementary Table 3 | Activation curve parameters of I_f current in sino-atrial node myocytes.

Mean activation curve parameters obtained in the different conditions indicated. Curves were measured in single cells (n= number of cells) as outlined in the Methods, fitted with the Boltzmann distribution equation and parameters were averaged. Values and symbols refer to the plots in Figure 3b and c (for c-di-GMP and 2'3'-cGAMP) and Figure 4h (for C11).

in pipette → ↓	**no cAMP**			**cAMP 10 µM**			**shift *vs* no cAMP (mV)**
	$V_{1/2}$ (mV)	**s (mV)**	**n**	**$V_{1/2}$ (mV)**	**s (mV)**	**n**	
control	-76.9±1.4	9.2±0.9	●, 9	-69.1±1.1	9.1±0.7	○, 8	7.8
c-di-GMP (100 µM)	-81.9±1.4	9.7±0.8	■, 8	-77.0±1.3	8.8±0.5	□,13	4.9
shift *vs* control (mV)	-5			-7.9			
control	-76±0.6	9.6±0.6	●, 5	-68.6±1.3	7.8±0.3	○, 4	7.4
2'3'-cGAMP (100 µM))	-81.3±0.8	10.1±0.7	♦, 6	-80.5±0.6	10.9±0.7	◊, 6	0.8
shift *vs* control (mV)	-5.3			-11.9			
control	-76.8±0.6	8.4±0.4	●, 15	-70.0±0.7	8.5±0.4	○, 9	6.8
C11 (100 µM)	-82.7±1.5	9.4±0.4	▲, 15	-82.4±2.4	8.7±0.5	Δ, 7	0.3
shift *vs* control (mV)	-5.9			-12.4			

Supplementary Figure 1

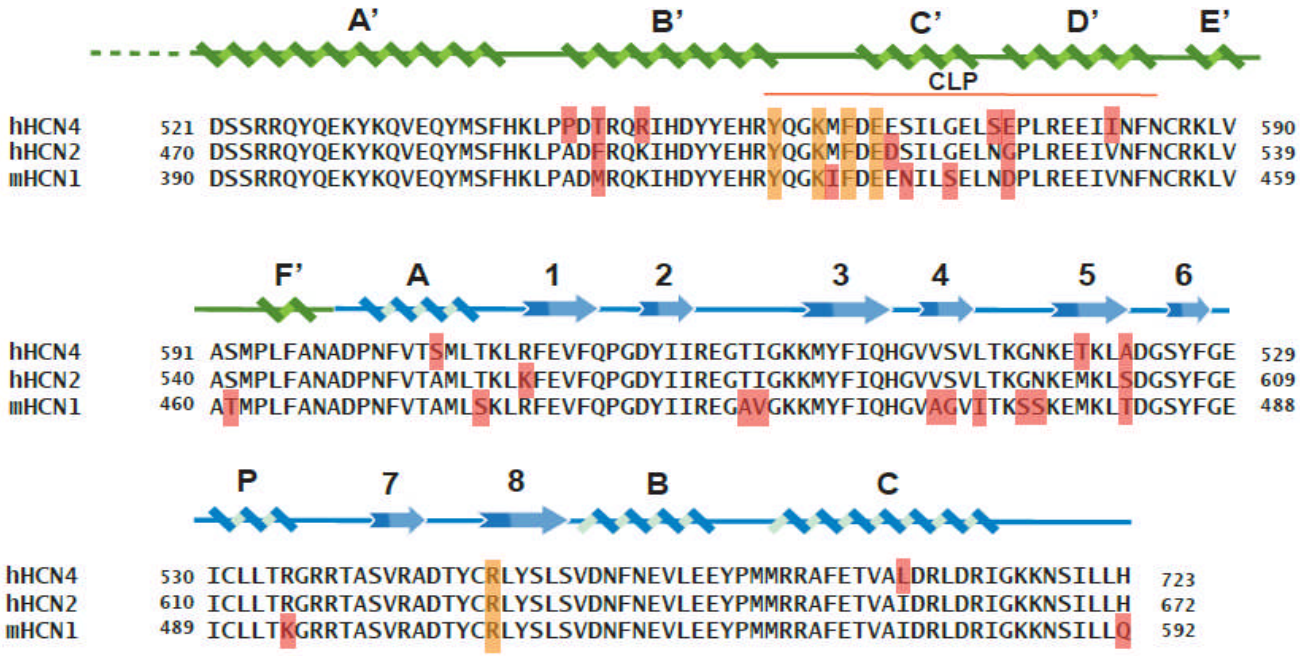

Supplementary Figure 2

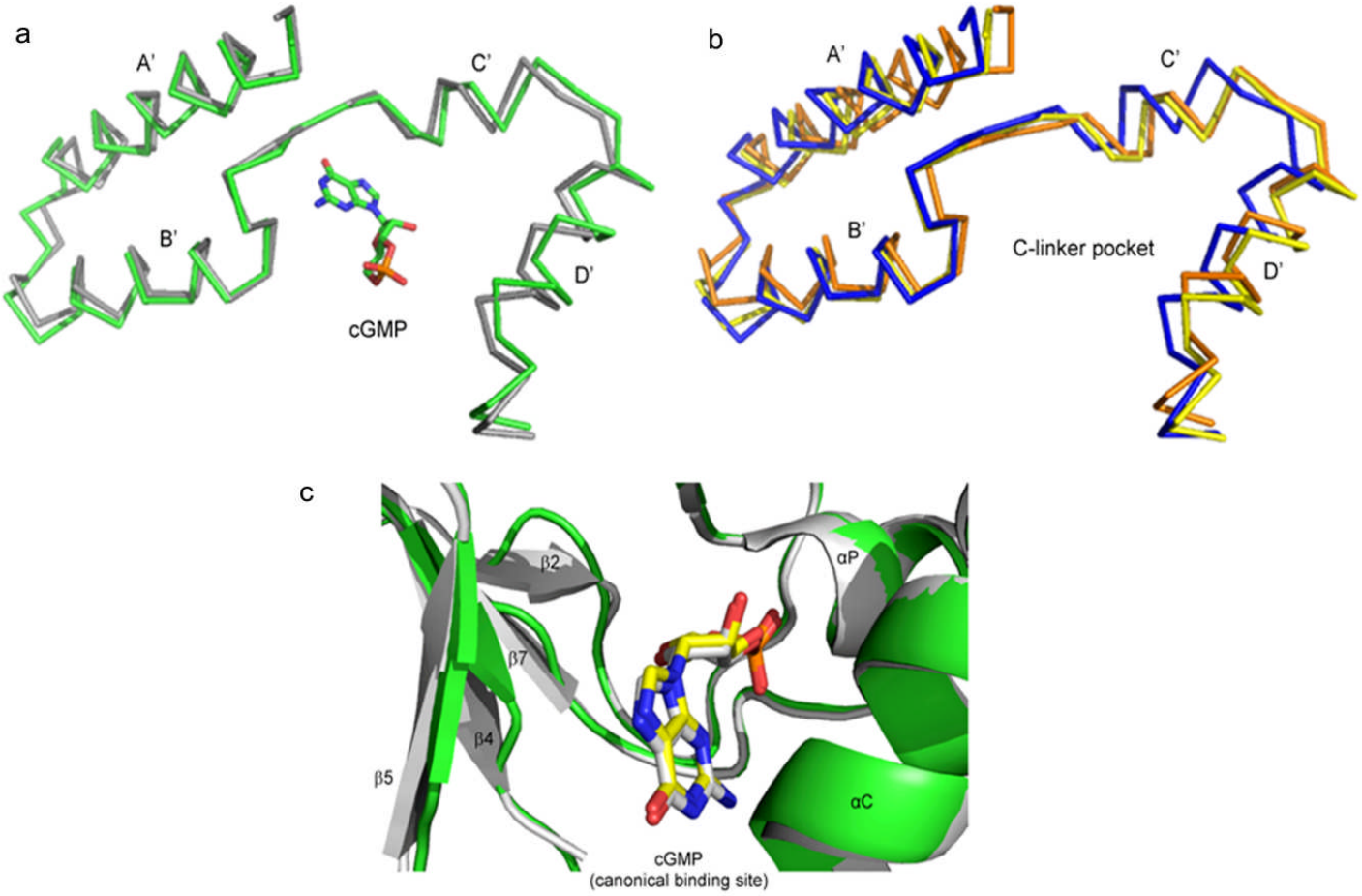

Supplementary Figure 3

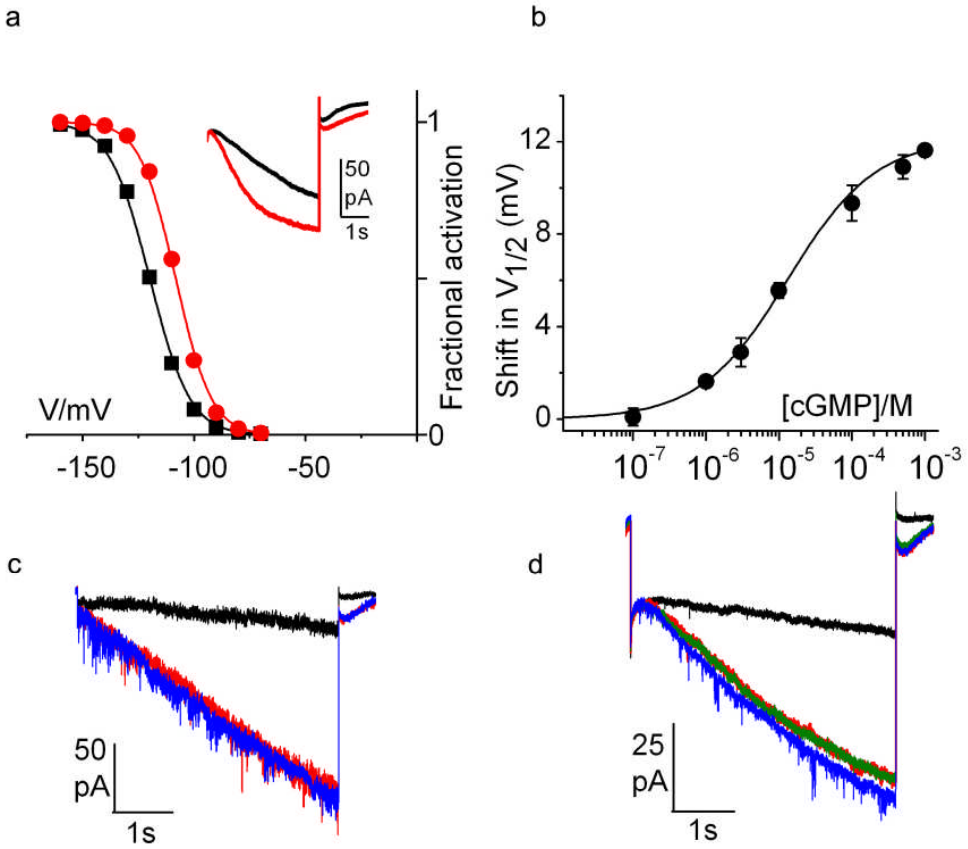

Supplementary Figure 4

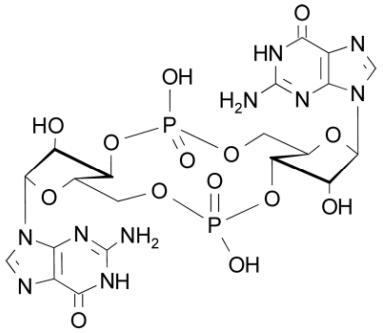

c-di-GMP

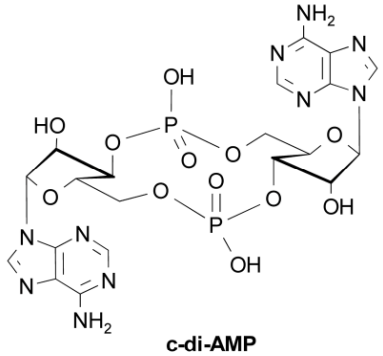

c-di-AMP

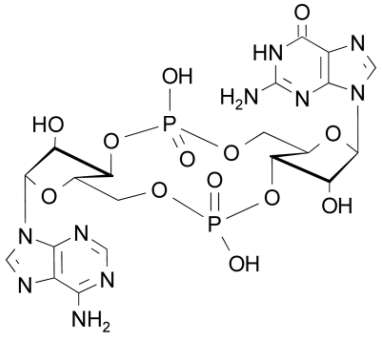

3′3′-cGAMP / c-[G(3',5')pA(3',5')p]

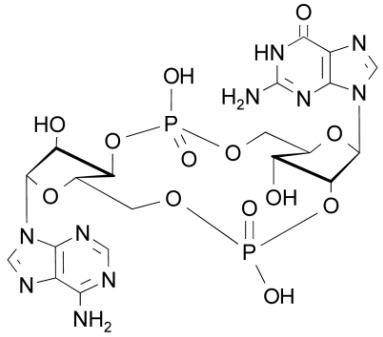

2'3'-cGAMP / c-[G(2',5')pA(3',5')p]

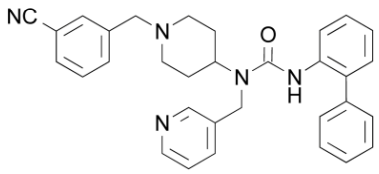

C11

Supplementary Figure 5

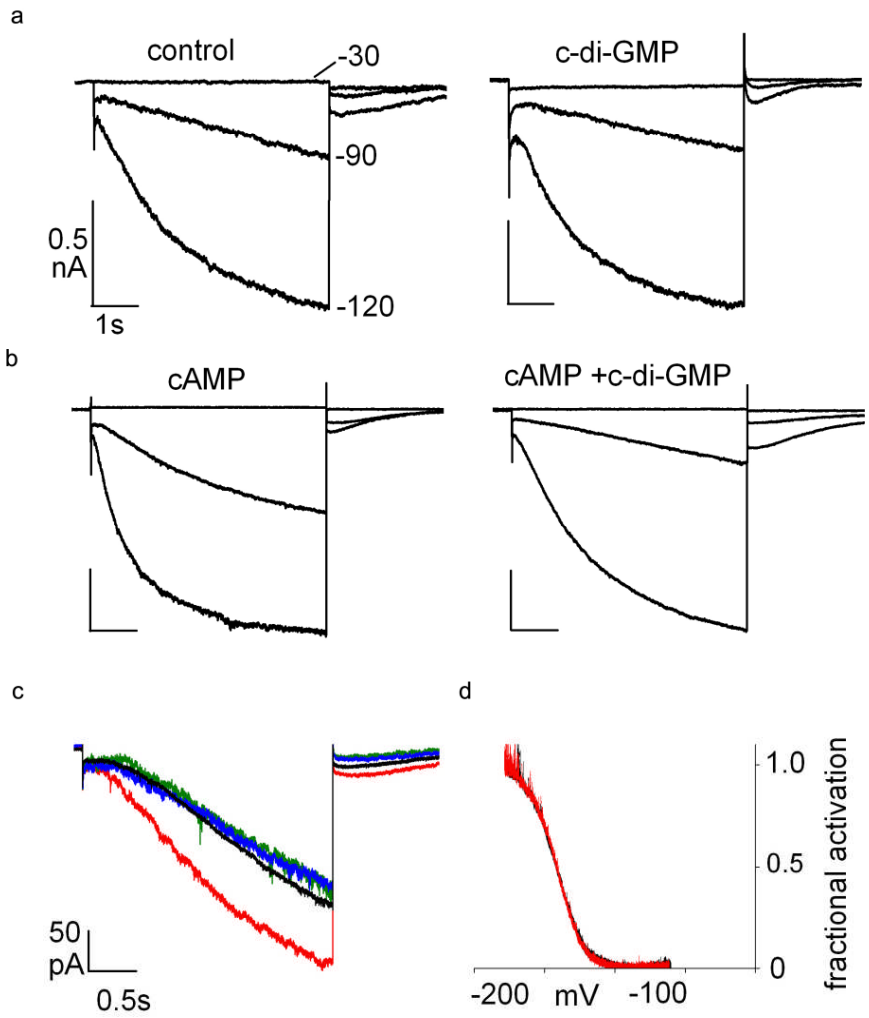

Supplementary Figure 6

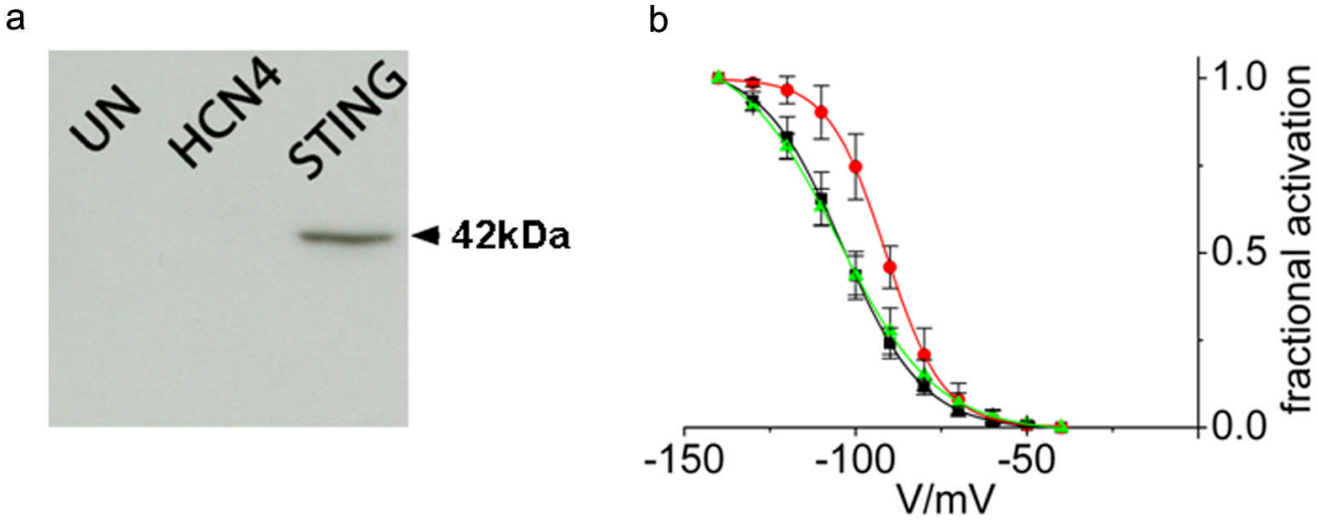

Supplementary Figure 7

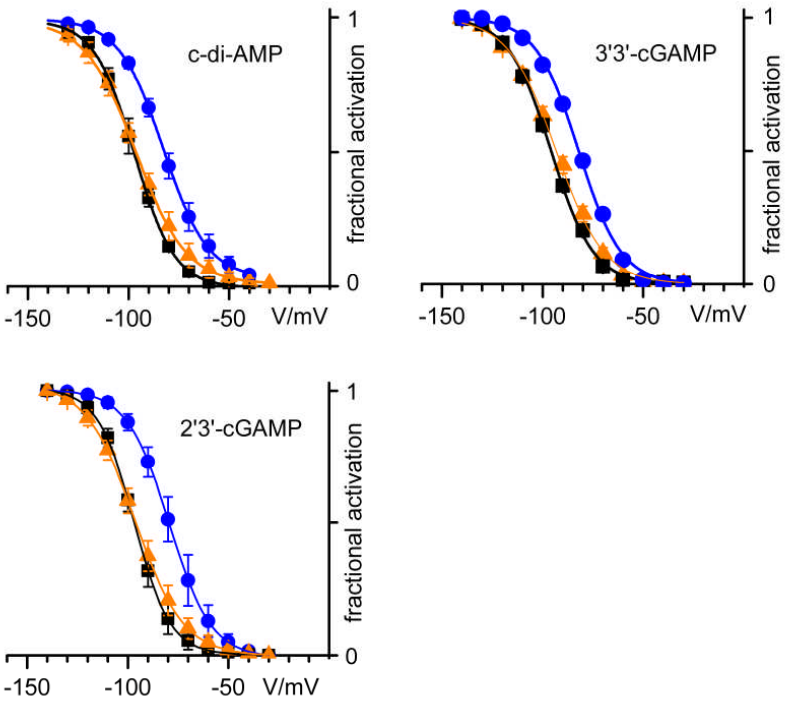

Supplementary Figure 8